

# Joint Activity Detection and Channel Estimation in Massive Machine-Type Communications with Low-Resolution ADC

Ye Xue<sup>1</sup>, An Liu<sup>2</sup>, Yang Li<sup>1</sup>, Qingjiang Shi<sup>1,3</sup>, and Vincent Lau<sup>4</sup>

<sup>1</sup> Shenzhen Research Institute of Big Data, Shenzhen 518172, China

<sup>2</sup> College of Information Science and Electronic Engineering, Zhejiang University, Hangzhou 310027, China

<sup>3</sup> Tongji University, Shanghai 201804, China

<sup>4</sup> Dept. of ECE, The Hong Kong University of Science and Technology, Hong Kong

**Abstract**—In massive machine-type communications, data transmission is usually considered sporadic, and thus inherently has a sparse structure. This paper focuses on the joint activity detection (AD) and channel estimation (CE) problems in massive-connected communication systems with low-resolution analog-to-digital converters. To further exploit the sparse structure in transmission, we propose a maximum posterior probability (MAP) estimation problem based on both sporadic activity and sparse channels for joint AD and CE. Moreover, a majorization-minimization-based method is proposed for solving the MAP problem. Finally, various numerical experiments verify that the proposed scheme outperforms state-of-the-art methods.

**Index Terms**—massive machine-type communications, activity detection, and channel estimation.

## I. INTRODUCTION

Future wireless networks will face a dramatically increasing density of devices, especially in massive machine-type communications (mMTC). This makes accurate activity detection (AD) and channel estimation (CE) very challenging due to the high-dimensional channel matrices and the limited number of pilots.

Fortunately, the sporadic transmission property [1] enables sparse recovery methods for AD and CE problems in mMTC [2]–[8]. Specifically, [2] explored the sparse structure of the active devices and proposed a modified Bayesian compressive sensing algorithm to perform joint AD and CE in cloud radio access networks. References [3]–[5] resorted to the message-passing-based method to estimate the sparse channel matrices and then detected the active devices by comparing the estimated channel power of each device in massive-connected systems. However, these works have the full-resolution assumption of the signal which prevents them from being deployed in practical systems with impairments. References [6]–[8] considered low-resolution analog-to-digital converters (ADC) in the system but they only exploited the sparsity from the sporadic activity, ignoring the sparsity in the angular domain channel. However, by further exploiting the angular

domain channel sparsity, it would be possible to improve the AD and CE performance.

In this paper, we jointly exploit the sparsity in the device activity and the angular domain channel to address the joint AD and CE problem in mMTC systems with low-resolution ADC. The main contributions are summarized below.

- **Hierarchical Joint Sparsity of Device Activity and Channel:** We consider joint group sparsity introduced by the sporadic device activity and the massive MIMO channel with a hierarchical sparsity structure<sup>1</sup>. To fully explore this structured sparsity, we propose a two-level hierarchical sparsity model. Such a model can accurately represent the joint sparsity as well as enable a tractable solution.
- **Maximum posterior probability (MAP)-based Problem Formulation with Bussgang Decomposition:** To solve the joint AD and CE problem, we start from the MAP estimation criterion. However, naive MAP formulation will lead to a non-elementary likelihood. To address this issue, we propose a likelihood based on the Bussgang decomposition [10]–[12]. The resultant likelihood is quadratic, which dramatically releases the computational burden.
- **Majorization-Minimization (MM)-based Algorithm Design:** We then propose to solve the MAP problem by MM-based method with a novel surrogate design. In each iteration, the proposed algorithm can be reduced to solving a quadratic sub-problem with the second-order coefficient matrix being diagonal.

*Notations:*  $\mathbf{X}^{-1}$ ,  $\mathbf{X}^T$ ,  $\mathbf{X}^*$  and  $\mathbf{X}^H$  denote the inverse, transpose, conjugate, and conjugate transpose of the matrix  $\mathbf{X}$ , respectively.  $Re(\mathbf{X})$  is the real-value decomposition of the complex matrix  $\mathbf{X}$ .  $Vec(\mathbf{X})$  is the vectorization of matrix  $\mathbf{X}$ .  $diag([a_1, \dots, a_N]^T)$  is the diagonal matrix with  $a_1, \dots, a_N$  being the diagonal elements. The notation  $\otimes$  is the Kronecker product. We use  $\mathcal{CN}(x; \mu, \nu)$  and  $\mathcal{N}(x; \mu, \nu)$  to denote the PDF of a complex Gaussian and a real Gaussian random variable  $x$  with mean  $\mu$  and variance  $\nu$ , respectively. The

The work of Y. Xue was supported by the National Key R&D Program of China under grant 2022YFA1003900. The work of Q. Shi was supported by the National Natural Science Foundation of China (NSFC) under grant 62231019. The work of Y. Li was supported by the NSFC under grant 62101349.

<sup>1</sup>An inactive device will lead to the corresponding column of the channel matrix being zero. On the other hand, the channel of an active device will exhibit burst sparsity induced by the scattering cluster [9], as illustrated in Fig. 1.

notation  $\mathbf{R}_{xy}$  is the correlation matrix of random vectors  $\mathbf{x}$  and  $\mathbf{y}$ .

## II. SYSTEM MODEL

### A. Uplink Signal Model

In this work, we consider a single-cell uplink system with an  $M$ -antenna base station (BS) ( $M \gg 1$ ) simultaneously serving  $N$  single-antenna devices. These  $N$  devices exhibit sporadic activity as shown in Fig.1.

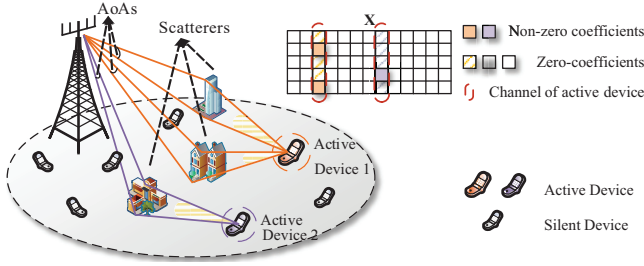


Fig. 1. Uplink system with both sparse device activities and sparse angular domain channels.

The activity of the  $n$ -th device in a particular time slot is given as

$$s_n = \begin{cases} 1, & \text{if the } n\text{-th device is active,} \\ 0, & \text{otherwise.} \end{cases} \quad (1)$$

When the  $n$ -th device is active, it transmits a pilot sequence with  $T$  symbols. Hence, the received signal  $\mathbf{Y} \in \mathbb{C}^{M \times T}$  at the BS is given by

$$\mathbf{Y} = \sum_{n=1}^N s_n \sqrt{g_n} \mathbf{h}_n \mathbf{d}_n^T + \mathbf{V} \quad (2)$$

$$= \mathbf{H} \mathbf{S} \mathbf{G}^{1/2} \mathbf{D} + \mathbf{V}.$$

In Eq.(2),  $\mathbf{h}_n \in \mathbb{C}^{M \times 1}$  represents the quasi-static small-scale fading channel between the  $n$ -th device and the BS, and  $\sqrt{g_n}$  is the effective power factor combining the path loss and transmit power of the  $n$ -th device, which is assumed to be known at the receiver.  $\mathbf{d}_n = [d_{n,1}, \dots, d_{n,T}] \in \mathbb{C}^{T \times 1}$  is the pilot signal assigned to the  $n$ -th device.  $\mathbf{V} \in \mathbb{C}^{M \times T}$  is the complex Gaussian noise matrix with zero mean and covariance matrix  $\sigma_v^2 \mathbf{I}$ . We also have  $\mathbf{H} = [\mathbf{h}_1, \dots, \mathbf{h}_N] \in \mathbb{C}^{M \times N}$ ,  $\mathbf{S} = \text{diag}([s_1, \dots, s_N]^T)$ ,  $\mathbf{G}^{1/2} = \text{diag}([\sqrt{g_1}, \dots, \sqrt{g_N}]^T)$  and  $\mathbf{D} = [\mathbf{d}_1, \dots, \mathbf{d}_N]^T \in \mathbb{C}^{N \times T}$ .

### B. Channel Sparsity in Angular Domain

We consider flat-fading massive MIMO channels with limited scatterers around the BS. Applying the widely used discrete multipath channel model in [9], the uplink channel response from the  $n$ -th device to the BS can be modeled as

$$\mathbf{h}_n = \sum_{c=1}^{N_c} \zeta_{c,n} \mathbf{u}(\theta^c), \quad (3)$$

where  $N_c$  is the number of scattering clusters,  $\zeta_{c,n}$  stands for the complex channel gain corresponding to the  $c$ -th scattering

cluster path of the  $n$ -th device,  $\theta^c$  represents the azimuth angle of arrival (AoA) corresponding to the  $c$ -th scattering cluster, and  $\mathbf{u}(\theta^c) \in \mathbb{C}^M$  is the steering vector for the BS antenna array. The number of the scattering clusters  $N_c$  is usually much smaller than the number of antennas  $M$  in the massive MIMO regime. Specifically, for a half-wavelength space uniform linear array (ULA), the steering vector has the form

$$\mathbf{u}(\theta) = \frac{1}{\sqrt{M}} \left[ 1, e^{-j\pi \sin(\theta)}, e^{-j2\pi \sin(\theta)}, \dots, e^{-j(M-1)\pi \sin(\theta)} \right]^T. \quad (4)$$

Let  $\{\theta_1, \dots, \theta_{\tilde{M}}\}$  be a uniform sampling grid, which covers the angular spread  $[-\frac{\pi}{2}, \frac{\pi}{2}]$ . We then define  $\mathbf{U}_R = [\mathbf{u}(\theta_1), \dots, \mathbf{u}(\theta_{\tilde{M}})] \in \mathbb{C}^{M \times \tilde{M}}$  and  $\tilde{\mathbf{H}} \in \mathbb{C}^{\tilde{M} \times N}$  as the array response matrix and the angular domain channel matrix, respectively. Then,  $\mathbf{H}$  can be expressed in a compact form as

$$\mathbf{H} = \mathbf{U}_R \tilde{\mathbf{H}}. \quad (5)$$

Note that the angular domain channel matrix  $\tilde{\mathbf{H}} \in \mathbb{C}^{\tilde{M} \times N}$  is, in general, sparse due to the limited local scattering effects at the BS side in massive MIMO systems [13].

Let  $\mathbf{X} = \tilde{\mathbf{H}} \mathbf{S}$  being the aggregated variable, the uplink signal model (2) can be expressed as

$$\mathbf{Y} = \mathbf{U}_R \tilde{\mathbf{H}} \mathbf{S} \mathbf{G}^{1/2} \mathbf{D} + \mathbf{V} \quad (6)$$

$$= \mathbf{U}_R \mathbf{X} \mathbf{G}^{1/2} \mathbf{D} + \mathbf{V}.$$

### C. Receiver with Low-Resolution ADC

At the BS, we consider the low-resolution ADC effect and focus on the scenario where the thermal noise in the system appears before the signal is quantized. Furthermore, we assume the received signal  $\mathbf{Y}$  is quantized component-wisely and separately to the real and imaginary parts with a general  $B$ -bit scalar quantizer (not necessarily the uniform quantizer). The signal after quantization is given by

$$\mathbf{R} = Q_B^c(\mathbf{Y}), \quad (7)$$

where  $Q_B^c(\cdot)$  is applied component-wise. Specifically, for each component, we have

$$Q_B^c(Y_{(m,n)}) = Q_B(\text{Re}\{Y_{(m,n)}\}) + jQ_B(\text{Im}\{Y_{(m,n)}\}). \quad (8)$$

Each real-valued  $B$ -bit scalar quantizer,  $Q_B$ , maps the real-valued input onto a finite-cardinal quantization alphabet  $\{\beta_{l_B} : \beta_1, \dots, \beta_{2^B}\}$  according to  $2^B - 1$  quantization thresholds:  $\{\alpha_{l_B} : -\infty < \alpha_1 < \alpha_2 < \dots < \alpha_{2^B-1} < \infty\}$ . We define  $\alpha_0 = -\infty$  and  $\alpha_{2^B} = \infty$  for notation convenience. The output of each real-valued scalar quantizer is  $\beta_{l_B}$  if the input belongs to the interval  $(\alpha_{l_B-1}, \alpha_{l_B}]$ . We further define  $\Delta_{l_B} = \beta_{l_B} - \beta_{l_B-1}$  as the quantization step size.

## III. MAP-BASED PROBLEM FORMULATION

The joint AD and CE is modeled as an MAP estimation problem with respect to the aggregated variable  $\mathbf{X}$  in this section. We shall first elaborate on the hierarchical prior

probability model on  $\mathbf{X}$ . Then we will present the likelihood approximation via Bussgang decomposition. Based on these two components, we will elaborate on the MAP formulation.

### A. Hierarchical Prior Probability of Aggregate Sparse Variable

The aggregated variable  $\mathbf{X} = \bar{\mathbf{H}}\mathbf{S}$  has two sources of sparsity, namely, the sparsity induced by the sporadic device activity  $\mathbf{S}$  and the group sparsity induced by the limited scattering in  $\bar{\mathbf{H}}$ . We will illustrate the prior of  $\mathbf{S}$  and  $\bar{\mathbf{H}}$  separately and then give the overall two-level hierarchical prior for  $\mathbf{X}$ .

1) *Prior for device activity  $\mathbf{S}$* : As illustrated in Section II,  $\mathbf{S} = \text{diag}([s_1, \dots, s_N]^T)$  represents the device activity with i.i.d. binary elements. Assume that we have knowledge of the device active ratio  $q_s$ . Then, the prior probability of the activity of the  $n$ -th MTC device is given by

$$p(s_n) = q_s^{s_n} (1 - q_s)^{1-s_n}. \quad (9)$$

2) *Prior for the angular domain channel  $\bar{\mathbf{H}}$* : Following the commonly used sparse Bayesian model [14], we assign a Gaussian prior distribution with distinct precision for each element of  $\bar{\mathbf{H}}$ . The prior of  $\bar{H}_{(m,n)}$  is given by

$$p(\bar{H}_{(m,n)}|\gamma_{(m,n)}) = \mathcal{CN}(\bar{H}_{(m,n)}; 0, \gamma_{(m,n)}^{-1}). \quad (10)$$

The precision  $\{\gamma_{(m,n)} : m = 1, \dots, M, n = 1, \dots, N\}$  is given by i.i.d. Gamma distribution

$$p(\gamma_{(m,n)}) = \Gamma(\gamma_{(m,n)}; a, b), \quad (11)$$

where  $a, b$  are the hyperparameters. With an appropriate choice of the hyperparameters  $a$  and  $b$ ,<sup>2</sup> the distribution  $p(\bar{H}_{(m,n)})$  is recognized as encouraging sparsity due to the heavy tails and sharp peak at zero [16]. The overall prior distribution of  $\bar{\mathbf{H}}_{(m,n)}$  is given by

$$\begin{aligned} p(\bar{H}_{(m,n)}) &= \int_{-\infty}^{\infty} p(\bar{H}_{(m,n)}|\gamma_{(m,n)})p(\gamma_{(m,n)})d\gamma_{(m,n)} \quad (12) \\ &= \frac{a}{\pi b} \left( \frac{\|\bar{H}_{(m,n)}\|^2}{b} + 1 \right)^{-(a+1)}. \end{aligned}$$

3) *Hierarchical prior for the aggregated variable  $\mathbf{X}$* : According to (9)–(12) and the relation  $\mathbf{X} = \bar{\mathbf{H}}\mathbf{S}$ , we have

$$\begin{aligned} p(\mathbf{X}) &= \prod_{n=1}^N \left( \left( p(s_n = 1) \prod_{m=1}^M p(X_{(m,n)}|s_n = 1) \right) \right. \\ &\quad \left. + \left( p(s_n = 0) \prod_{m=1}^M p(X_{(m,n)}|s_n = 0) \right) \right). \quad (13) \end{aligned}$$

In Eq. (13), we have  $p(X_{(m,n)}|s_n = 1) = p(\bar{H}_{(m,n)})$  and  $p(X_{(m,n)}|s_n = 0) = \delta(X_{(m,n)})$ . To avoid the undesirable

singularity of  $\delta(\cdot)$ , we consider the following approximation of  $\delta(X_{(m,n)})$ :

$$p(X_{(m,n)}|s_n = 0) = \mathcal{CN}(X_{(m,n)}; 0, \epsilon), \quad (14)$$

where  $\epsilon$  is a very small value.

As such, the logarithmic prior of  $\mathbf{X}$  is given by

$$\begin{aligned} \log p(\mathbf{X}) &= \log p(\mathbf{x}) = \sum_{n=1}^N \log \left[ \sum_{s_n \in \{0,1\}} \left( (1 - q_s) \right. \right. \\ &\quad \left. \left. \times \frac{1}{(\pi\epsilon)^M} \prod_{i_r=(n-1)M+1}^{nM} \exp\left(-\frac{x_{i_r}^2 + x_{i_r+MN}^2}{\epsilon}\right) \right)^{1-s_n} \right. \\ &\quad \left. \times \left( q_s \left(\frac{a}{\pi b}\right)^M \prod_{i_r=(n-1)M+1}^{nM} \left(\frac{x_{i_r}^2 + x_{i_r+MN}^2}{b} + 1\right)^{-(a+1)} \right)^{s_n} \right] \quad (15) \end{aligned}$$

where  $\mathbf{x} \triangleq \text{Re}(\text{Vec}(\mathbf{X}))$ .

### B. Approximation of the Likelihood Function via Bussgang Decomposition

Another important component in the MAP formulation is the likelihood function  $p(\mathbf{R}|\mathbf{X})$ . Due to the quantization, writing  $p(\mathbf{R}|\mathbf{X})$  in a direct way [17]–[19] will result in a very complicated and highly non-linear function, which will lead to difficult optimization and numerical issues. To address these drawbacks, we adopt the Bussgang decomposition [10] to model the quantization effect in the derivation of the likelihood function. By the Bussgang decomposition, the likelihood can be approximated by a Gaussian likelihood, which leads to a more tractable optimization problem.

For mathematical convenience, we first reformat  $\mathbf{Y}$  in Eq. (6) into a real-valued vector. The real-valued receive signal after vectorization is given by

$$\mathbf{r} = Q_B^c(\mathbf{y}) = Q_B^c(\tilde{\Phi}\mathbf{x} + \mathbf{v}), \quad (16)$$

where  $\mathbf{y} = \text{Re}(\text{Vec}(\mathbf{Y})) \in \mathbb{R}^{2MT}$ ,  $\tilde{\Phi} = \text{Re}(\text{Vec}(\mathbf{G}^{1/2}\mathbf{D})^T \otimes \mathbf{U}_R) \in \mathbb{R}^{2MT \times 2MN}$ ,  $\mathbf{x} = \text{Re}(\text{Vec}(\mathbf{X})) \in \mathbb{R}^{2MN}$  and  $\mathbf{v} = \text{Re}(\text{Vec}(\mathbf{V})) \in \mathbb{R}^{2MT}$ . Then, using Bussgang decomposition [10], the received signal after quantization can be expressed as

$$\mathbf{r} \cong \mathbf{K}\tilde{\Phi}\mathbf{x} + \mathbf{K}\mathbf{v} + \mathbf{n}_q = \mathbf{A}\mathbf{x} + \mathbf{z}, \quad (17)$$

where  $\cong$  means equivalent upto the second-order statistics,  $\mathbf{K} = \mathbf{R}_{ry}\mathbf{R}_{yy}^{-1}$ ,  $\mathbf{A} = \mathbf{K}\tilde{\Phi}$ , and  $\mathbf{z} = \mathbf{K}\mathbf{v} + \mathbf{n}_q$  is the effective noise. The correlation matrix of the residual noise  $\mathbf{n}_q$  in Bussgang decomposition is  $\mathbf{R}_{\mathbf{n}_q\mathbf{n}_q} = \mathbf{R}_{rr} - \mathbf{K}\mathbf{R}_{yy}\mathbf{K}^H$ . Therefore, the covariance matrix of  $\mathbf{z}$  is given by

$$\Sigma = \frac{\sigma_v^2}{2} \mathbf{K}\mathbf{K}^T + \mathbf{R}_{\mathbf{n}_q\mathbf{n}_q}. \quad (18)$$

<sup>2</sup>In this paper, we set  $a, b \rightarrow 0$  as in [15] to obtain a broad hyperprior.

Then, the log-likelihood function is then given by<sup>3</sup>

$$\log p(\mathbf{r}|\mathbf{x}) = -\frac{1}{2}(\mathbf{r} - \mathbf{A}\mathbf{x})^T \boldsymbol{\Sigma}^{-1}(\mathbf{r} - \mathbf{A}\mathbf{x}) \quad (19)$$

$$- \log \sqrt{(2\pi)^{2MT} \det(\boldsymbol{\Sigma})}$$

Combining the results of the log prior distribution  $p(\mathbf{x})$  in (15) and the log-likelihood  $p(\mathbf{r}|\mathbf{x})$  in (19), the MAP problem is formulated as

$$\underset{\mathbf{x} \in \mathbb{R}^{2MN}}{\text{minimize}} \quad f(\mathbf{x}), \quad (20)$$

where  $f(\mathbf{x}) = -\log p(\mathbf{r}|\mathbf{x}) - \log p(\mathbf{x}) \propto -\log p(\mathbf{x}|\mathbf{r})$ .

#### IV. MM-BASED ALGORITHM FOR JOINT AD AND CE

##### A. MM-based Estimation of the Aggregated Variable

In this section, we adopt an MM-based method to iteratively find a stationary point of the non-convex problem (20). The MM-based algorithm requires an effective surrogate function. To design the surrogate function, we need the following lemma:

**Lemma 1.** [Majorization of a Quadratic Form] Let  $\boldsymbol{\Omega} \in \mathbb{R}^{L \times L}$  be a symmetric positive semi-definite matrix. Then the quadratic form  $\mathbf{x}^T \boldsymbol{\Omega} \mathbf{x}$  is majorized by  $\mathbf{x}^T \tilde{\boldsymbol{\Omega}} \mathbf{x} - 2\mathbf{x}^T (\tilde{\boldsymbol{\Omega}} - \boldsymbol{\Omega}) \mathbf{x}_0 + \mathbf{x}_0^T (\tilde{\boldsymbol{\Omega}} - \boldsymbol{\Omega}) \mathbf{x}_0$ , with  $\tilde{\boldsymbol{\Omega}} \succeq \boldsymbol{\Omega}$ , where  $\mathbf{x}_0 \in \mathbb{R}^L$  is any fixed point.

*Proof:*  $(\mathbf{x} - \mathbf{x}_0)^T (\tilde{\boldsymbol{\Omega}} - \boldsymbol{\Omega})(\mathbf{x} - \mathbf{x}_0) \geq 0, \forall \mathbf{x}$  given  $\mathbf{x}_0$ . ■

We apply the expectation–maximization procedure and the Taylor expansion of  $-\log P(\mathbf{x})$  to deal with the non-convexity issue, and apply Lemma 1 to simplify the surrogate function. At the  $j$ -th iteration, the surrogate function is given by

$$\hat{f}(\mathbf{x}|\mathbf{x}^{(j)}) \quad (21)$$

$$= \frac{1}{2} \mathbf{x}^T \mathbf{J} \mathbf{x} - \mathbf{x}^T (\mathbf{J} - \mathbf{A}^T \boldsymbol{\Sigma}^{-1} \mathbf{A}) \mathbf{x}^{(j)} - \mathbf{x}^T \mathbf{A}^T \boldsymbol{\Sigma}^{-1} \mathbf{r}$$

$$+ \sum_{n=1}^N \left( \langle \lambda_{0\mathbf{x}^{(j)}}[n] \rangle \sum_{i_r=(n-1)M+1}^{nM} \frac{x_{i_r}^2 + x_{i_r+MN}^2}{\epsilon} \right.$$

$$\left. + \langle \lambda_{1\mathbf{x}^{(j)}}[n] \rangle (1+a) \sum_{i_r=(n-1)M+1}^{nM} \left( \frac{x_{i_r}^2 + x_{i_r+MN}^2}{b \left( \frac{(x_{i_r}^{(j)})^2 + (x_{i_r+MN}^{(j)})^2}{b} + 1 \right)} \right) \right)$$

$$+ g_1(\mathbf{x}^{(j)})$$

$$= \frac{1}{2} \mathbf{x}^T \mathbf{J} \mathbf{x} - \mathbf{x}^T (\mathbf{J} - \mathbf{A}^T \boldsymbol{\Sigma}^{-1} \mathbf{A}) \mathbf{x}^{(j)} - \mathbf{x}^T \mathbf{A}^T \boldsymbol{\Sigma}^{-1} \mathbf{r} + \mathbf{x}^T \boldsymbol{\Lambda}_0^{(j)} \mathbf{x}$$

$$+ \mathbf{x}^T \boldsymbol{\Lambda}_1^{(j)} \odot \mathbf{W}^{(j)} \mathbf{x} + g(\mathbf{x}^{(j)}),$$

where we have  $\mathbf{J} = \lambda_{max}(\mathbf{A}^T \boldsymbol{\Sigma}^{-1} \mathbf{A}) \mathbf{I}$ , with  $\lambda_{max}(\mathbf{A}^T \boldsymbol{\Sigma}^{-1} \mathbf{A})$  being the largest eigenvalue of  $\mathbf{A}^T \boldsymbol{\Sigma}^{-1} \mathbf{A}$ .  $\mathbf{A} \in \mathbb{R}^{2MT \times 2MN}$  and  $\boldsymbol{\Sigma} \in \mathbb{R}^{2MT \times 2MT}$  are given by Eq.

(17) and Eq. (18), respectively. We also have

$$\langle \lambda_{0\mathbf{x}^{(j)}}[n] \rangle = \frac{(1-q_s)P_0(\mathbf{x}^{(j)}[n])}{(1-q_s)P_0(\mathbf{x}^{(j)}[n]) + (q_s)P_1(\mathbf{x}^{(j)}[n])}, \quad (22)$$

$$\langle \lambda_{1\mathbf{x}^{(j)}}[n] \rangle = \frac{(q_s)P_1(\mathbf{x}^{(j)}[n])}{(1-q_s)P_0(\mathbf{x}^{(j)}[n]) + (q_s)P_1(\mathbf{x}^{(j)}[n])}, \quad (23)$$

with

$$P_0(\mathbf{x}^{(j)}[n]) = \frac{1}{(\pi\epsilon)^M} \prod_{i_r=(n-1)M+1}^{nM} \exp\left(-\frac{(x_{i_r}^{(j)})^2 + (x_{i_r+MN}^{(j)})^2}{\epsilon}\right),$$

$$P_1(\mathbf{x}^{(j)}[n]) = \left(\frac{a}{\pi b}\right)^M \prod_{i_r=(n-1)M+1}^{nM} \left(\frac{(x_{i_r}^{(j)})^2 + (x_{i_r+MN}^{(j)})^2}{b} + 1\right)^{-(a+1)},$$

and  $\mathbf{x}^{(j)}[n] = [x_{(n-1)M+1}^{(j)}, \dots, x_{(N+n)M}^{(j)}]^T$ .  $\boldsymbol{\Lambda}_0^{(j)} \in \mathbb{R}^{2MN}$ ,  $\boldsymbol{\Lambda}_1^{(j)} \in \mathbb{R}^{2MN}$ , and  $\mathbf{W}^{(j)} \in \mathbb{R}^{2MN}$  are diagonal matrices with the diagonal elements given in Table I, where  $\mathcal{V}(n) = \{i : i = (n-1)M+1, \dots, nM, MN+(n-1)M+1, \dots, (N+n)M\}$  is the index set of  $\mathbf{x}$  related to the  $n$ -th MTC device.

TABLE I  
VALUES OF PARAMETERS IN (24)

| Parameters                            | Values  |
|---------------------------------------|---|
| $\boldsymbol{\Lambda}_{0(i,i)}^{(j)}$ | $i \in \mathcal{V}(n)$<br>$\frac{\langle \lambda_{0\mathbf{x}^{(j)}}[n] \rangle}{\epsilon}$ |
| $\boldsymbol{\Lambda}_{1(i,i)}^{(j)}$ | $i \in \mathcal{V}(n)$<br>$\frac{(1+a)\langle \lambda_{1\mathbf{x}^{(j)}}[n] \rangle}{b}$   |
| $\mathbf{W}_{i,i}^{(j)}$              | $i \leq MN$<br>$1/\left(\frac{(x_i^{(j)})^2 + (x_{i+MN}^{(j)})^2}{b} + 1\right)$            |
|                                       | $MN < i \leq 2MN$<br>$1/\left(\frac{(x_i^{(j)})^2 + (x_{i-MN}^{(j)})^2}{b} + 1\right)$      |

By dropping the constant and irrelevant terms in (21), the updated rule of  $\mathbf{x}^{(j+1)}$  is given by

$$\mathbf{x}^{(j+1)} \quad (24)$$

$$= \arg \min \frac{1}{2} \mathbf{x}^T \mathbf{J} \mathbf{x} - \mathbf{x}^T (\mathbf{J} - \mathbf{A}^T \boldsymbol{\Sigma}^{-1} \mathbf{A}) \mathbf{x}^{(j)}$$

$$- \mathbf{x}^T \mathbf{A}^T \boldsymbol{\Sigma}^{-1} \mathbf{r} + \mathbf{x}^T \boldsymbol{\Lambda}_0^{(j)} \mathbf{x} + \mathbf{x}^T \boldsymbol{\Lambda}_1^{(j)} \odot \mathbf{W}^{(j)} \mathbf{x}$$

$$= [(\mathbf{J} - \mathbf{A}^T \boldsymbol{\Sigma}^{-1} \mathbf{A}) \mathbf{x}^{(j)} + \mathbf{A}^T \boldsymbol{\Sigma}^{-1} \mathbf{r}]$$

$$\times (\mathbf{J} + 2\boldsymbol{\Lambda}_0^{(j)} + 2\boldsymbol{\Lambda}_1^{(j)} \odot \mathbf{W}^{(j)})^{-1}.$$

Algorithm 1 summarizes the key steps of the overall solution to recover the aggregated variable from Problem (20). Due to the page limit, we omit the convergence analysis. However, the convergence of the sequence (24) to the stationary point of Problem (20) can be established easily by checking the requirements of MM surrogate [22].

##### B. Activity Detection and Channel Estimation

After obtain  $\hat{\mathbf{x}}$  by Algorithm 1, the MAP estimator of the device activity  $s_n$  is given by

<sup>3</sup>Since Gaussian noise is the worst-case noise with respect to reducing information [11], [20], [21], we can approximate the likelihood function  $p(\mathbf{r}|\mathbf{x})$  by assuming  $\mathbf{n}_q$  is Gaussian.

---

**Algorithm 1** The Proposed MM-based Algorithm
 

---

- 1: **Input:**  $\mathbf{r}$ , measurement matrix  $\Phi$ , and noise variance  $\sigma_v^2$ .
  - 2: **Output:**  $\hat{\mathbf{x}}$
  - 3: **Initialize:**  $\mathbf{x}^{(0)} = \mathbf{0}$ ,  $j = 0$ .
  - 4: **Pre-computing:**
  - 5: **% Calculate coefficients in terms of Bussgang decomposition**
  - 6: 1: Calculate  $\mathbf{R}_{n_q n_q}$ ,  $\mathbf{K}$ .
  - 7: 2:  $\mathbf{A} = \mathbf{K}\Phi$ ,  $\Sigma = \sigma_v^2 \mathbf{K}\mathbf{K}^T + \mathbf{R}_{n_q n_q}$ ,  $\Omega_1 = \mathbf{A}^T \Sigma^{-1}$ ,  $\Omega_2 = \mathbf{A}^T \Sigma^{-1} \mathbf{A}$ ,  $\mathbf{f} = \Omega_1 \mathbf{r}$ ,  $\mathbf{J} = \lambda_{max}(\Omega_2) \mathbf{I}$ .
  - 8: **Iteration Estimation:**
  - 9: **% MM-based solver for estimation of  $\mathbf{x}$**
  - 10: **while** not converge **do**
  - 11: 3: Calculate  $\Lambda_0^{(j)}$ ,  $\Lambda_1^{(j)}$  and  $\mathbf{W}^{(j)}$  via (22), (23) and Table I.
  - 12: 4: Calculate  $\mathbf{x}^{(j+1)} = [(\mathbf{J} - \Omega_2)\mathbf{x}^{(j)} + \mathbf{f}][\mathbf{J} + 2\Lambda_0^{(j)} + 2\Lambda_1^{(j)} \odot \mathbf{W}^{(j)}]^{-1}$ .
  - 13: 5:  $j = j + 1$ .
  - 14: **end while**
  - 15: 6:  $\hat{\mathbf{x}} = \mathbf{x}^{(j+1)}$ .
- 

$$\hat{s}_n = \begin{cases} 1, & -(1+a) \sum_{i_r=(n-1)M+1}^{nM} (\log(\frac{\hat{x}_{i_r}^2 + \hat{x}_{i_r+MN}^2}{b} + 1) \\ & + \frac{\hat{x}_{i_r}^2 + \hat{x}_{i_r+MN}^2}{\epsilon}) > \varpi_{th}, \\ 0, & \text{otherwise,} \end{cases} \quad (25)$$

with  $\varpi_{th} = -\log q_s - M \log(\frac{a}{\pi b}) + \log(1 - q_s) + M \log \frac{1}{(\pi \epsilon)}$ .

Finally, we have  $\hat{\mathbf{S}} = \text{diag}([\hat{s}_1, \dots, \hat{s}_N]^T)$  and  $\hat{\mathbf{X}}$  can be obtained by reformatting  $\hat{\mathbf{x}}$ .

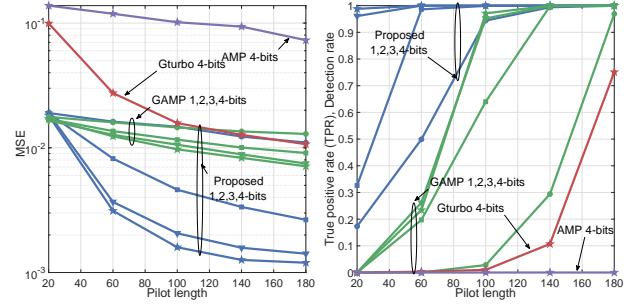
### C. Complexity Analysis

Algorithm 1 works for any general pilot. The computation cost is dominated by the calculation of the inverse of matrix  $\Sigma$  and the maximum eigenvalue of  $\Omega_2$ . However, if the pilot is chosen such that  $\mathbf{D}^H \mathbf{D}$  is diagonal or the diagonal elements dominate the off-diagonal ones,  $\Sigma$  and  $\Omega_2$  are diagonal or can be well-approximated by diagonal elements.<sup>4</sup> In this case, the dominant complexity of Algorithm 1 can be reduced to  $\mathcal{O}((NM)^2)$ . This is because the calculation in the matrix inversion and eigenvalue can be dramatically reduced by the diagonal approximation of  $\Sigma$  and the most complicated computation is the matrix-vector product at each iteration (line 4 in Algorithm 1). In addition, the proposed algorithm only involves the calculations of elementary functions in each iteration.

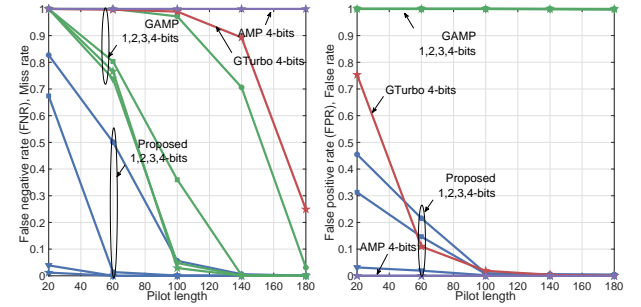
## V. NUMERICAL SIMULATION AND RESULTS DISCUSSION

In this section, we verify the performance of the proposed joint AD and CE method. We consider a scenario where  $N = 200$  online MTC devices are uniformly distributed in a single BS cell with radius  $R = 1$  km, and the device active ratio is  $q_s = 0.1$ . The large-scale fading of the  $n$ -th MTC device is  $10^{-12.81-3.67 \log_{10}(c_n)}$ , with  $c_n$  denoting the distance between the BS and the  $n$ -th device. The channel is generated by the widely used LTE spatial channel model (SCM) [23] with half-wavelength space ULA and  $M = 128$ . The SNR in

<sup>4</sup>All pilot matrices with sub-Gaussian property can easily satisfy this condition.



(a) Left: MSE versus pilot length. Right: TPR versus pilot length.



(b) Left: FNR versus pilot length. Right: FPR versus pilot length.

Fig. 2. Performance comparison with different pilot lengths. Set SNR=10 dB, and the pilot sequence is i.i.d. QPSK.

the simulations is the received SNR averaged over all devices, and the quantization scheme is the optimum quantizer given in [24]. The AD and CE performance of the proposed method is compared with AMP method [5], Hybrid GAMP method [25], and GTurbo method [18].

The performance metric for CE is the estimation mean squared error (MSE), which is defined as

$$\text{MSE} \triangleq \frac{\|\hat{\mathbf{x}} - \mathbf{x}\|_2^2}{2NM}. \quad (26)$$

To evaluate the AD performance, we compare the true positive rate (TPR)  $\triangleq \frac{\sum_{n=1}^N \mathbf{1}(\hat{s}_n=1|s_n=1)}{\sum_{n=1}^N \mathbf{1}(s_n=1)}$ , false negative rate (FNR)  $\triangleq \frac{\sum_{n=1}^N \mathbf{1}(\hat{s}_n=0|s_n=1)}{\sum_{n=1}^N \mathbf{1}(s_n=1)}$ , and false positive rate (FPR)  $\triangleq \frac{\sum_{n=1}^N \mathbf{1}(\hat{s}_n=1|s_n=0)}{\sum_{n=1}^N \mathbf{1}(s_n=0)}$ , which can be regarded as the probability of successful detection, missing detection, and false detection, respectively [26].

### A. Impact of Pilot Length

First, we compare the performance of different approaches under different pilot lengths in Fig. 2. Specifically, Fig. 3(a) shows the MSE and TPR performance, Fig. 3(b) shows the FNR and FPR performance. As shown in the results, the proposed method can achieve better performance with fewer pilots compared with the baselines. This is because the proposed method incorporates joint activity sparsity and angular channel sparsity.

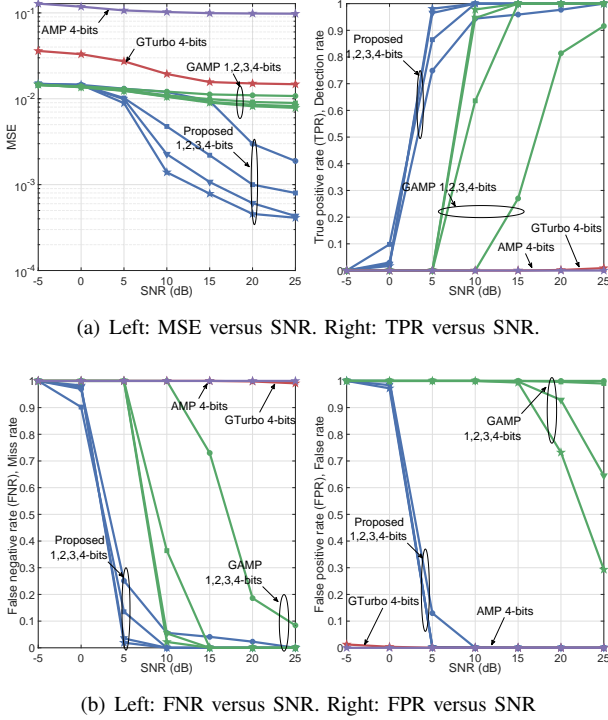


Fig. 3. Performance comparison with different SNRs. Here the pilot sequence is i.i.d. QPSK of the length  $T = 100$ .

### B. Impact of SNR

We also compare the performance under different SNRs in Fig. 3. The results show that the quantization effect is significant when the SNR is higher ( $> 5$  dB). In the low SNR region, the resolution of the ADC will not affect the performance, while in the high SNR region, the proposed method can achieve better performance with low-resolution ADC.

## VI. CONCLUSIONS

In this paper, we propose a new scheme for the mMTC system with low-resolution ADC to effectively detect the active devices and estimate the corresponding channels. By incorporating the joint device activity and angular channel sparsity, an MAP optimization problem is formed and an efficient MM-based algorithm is given to solve the MAP problem. The proposed scheme has no limitation to any specific pilot. Our simulation results demonstrate that the proposed method outperforms state-of-the-art schemes.

## REFERENCES

- [1] F. Boccardi, R. W. Heath, A. Lozano, T. L. Marzetta, and P. Popovski, "Five disruptive technology directions for 5G," *IEEE Commun. Mag.*, vol. 52, no. 2, pp. 74–80, 2014.
- [2] X. Xu, X. Rao, and V. K. Lau, "Active user detection and channel estimation in uplink CRAN systems," in *IEEE Int. Conf. Commun. (ICC)*, pp. 2727–2732, IEEE, 2015.
- [3] G. Hannak, M. Mayer, A. Jung, G. Matz, and N. Goertz, "Joint channel estimation and activity detection for multiuser communication systems," in *IEEE Int. Conf. Commun. Workshop (ICCW)*, pp. 2086–2091, IEEE, 2015.

- [4] L. Liu and W. Yu, "Massive connectivity with massive MIMO—part I: Device activity detection and channel estimation," *IEEE Trans. Signal Process.*, vol. 66, no. 11, pp. 2933–2946, 2018.
- [5] Z. Chen, F. Söhrabi, and W. Yu, "Sparse activity detection for massive connectivity," *IEEE Trans. Signal Process.*, vol. 66, no. 7, pp. 1890–1904, 2018.
- [6] T. Liu, S. Jin, C.-K. Wen, M. Matthaiou, and X. You, "Generalized channel estimation and user detection for massive connectivity with mixed-adc massive mimo," *IEEE Trans. Wireless Commun.*, vol. 18, no. 6, pp. 3236–3250, 2019.
- [7] S. Liu, H. Zhang, and Q. Zou, "Decentralized channel estimation for the uplink of grant-free massive machine-type communications," *IEEE Trans. Commun.*, vol. 70, no. 2, pp. 967–979, 2022.
- [8] Q. Zou, H. Zhang, D. Cai, and H. Yang, "Message passing based joint channel and user activity estimation for uplink grant-free massive mimo systems with low-precision adcs," *IEEE Signal Processing Letters*, vol. 27, pp. 506–510, 2020.
- [9] D. Tse and P. Viswanath, *Fundamentals of Wireless Communication*. Cambridge University Press, 2005.
- [10] J. Bussgang, "Crosscorrelation functions of amplitude-distorted Gaussian signals," 1952.
- [11] Y. Li, C. Tao, G. Seco-Granados, A. Mezghani, A. L. Swindlehurst, and L. Liu, "Channel estimation and performance analysis of one-bit massive MIMO systems," *IEEE Trans. Signal Process.*, vol. 65, no. 15, pp. 4075–4089, 2017.
- [12] S. Jacobsson, G. Durisi, M. Coldrey, T. Goldstein, and C. Studer, "Quantized precoding for massive MU-MIMO," *IEEE Trans. Commun.*, vol. 65, no. 11, pp. 4670–4684, 2017.
- [13] Y. Zhou, M. Herdin, A. M. Sayeed, and E. Bonek, "Experimental study of MIMO channel statistics and capacity via the virtual channel representation," *Univ. Wisconsin-Madison, Madison, WI, USA, Tech. Rep.*, vol. 5, pp. 10–15, 2007.
- [14] M. E. Tipping, "Sparse Bayesian learning and the relevance vector machine," *Journal of Machine Learning Research*, vol. 1, no. Jun, pp. 211–244, 2001.
- [15] J. Dai, A. Liu, and V. K. N. Lau, "FDD massive MIMO channel estimation with arbitrary 2D-array geometry," *IEEE Trans. Signal Process.*, vol. 66, pp. 2584–2599, May 2018.
- [16] S. Ji, Y. Xue, L. Carin, et al., "Bayesian compressive sensing," *IEEE Transactions on Signal Processing*, vol. 56, no. 6, p. 2346, 2008.
- [17] J. Mo, P. Schniter, and R. W. Heath, "Channel estimation in broadband millimeter wave MIMO systems with few-bit ADCs," *IEEE Trans. Signal Process.*, vol. 66, no. 5, pp. 1141–1154, 2018.
- [18] T. Liu, S. Jin, C. Wen, M. Matthaiou, and X. You, "Generalized channel estimation and user detection for massive connectivity with mixed-ADC massive MIMO," *IEEE Trans. Wireless Commun.*, vol. 18, no. 6, pp. 3236–3250, 2019.
- [19] C. Wen, C. Wang, S. Jin, K. Wong, and P. Ting, "Bayes-optimal joint channel-and-data estimation for massive MIMO with low-precision ADCs," *IEEE Trans. Signal Process.*, vol. 64, no. 10, pp. 2541–2556, 2016.
- [20] B. Hassibi and B. Hochwald, "How much training is needed in multiple-antenna wireless links?," *IEEE Trans. Inf. Theory*, vol. 49, no. 4, pp. 951–963, 2003.
- [21] S. N. Diggavi and T. M. Cover, "The worst additive noise under a covariance constraint," *IEEE Trans. Inf. Theory*, vol. 47, no. 7, pp. 3072–3081, 2001.
- [22] Y. Sun, P. Babu, and D. P. Palomar, "Majorization-minimization algorithms in signal processing, communications, and machine learning," *IEEE Trans. Signal Process.*, vol. 65, no. 3, pp. 794–816, 2017.
- [23] J. Salo, G. Del Galdo, J. Salmi, P. Kyösti, M. Milojevic, D. Laselva, and C. Schneider, "Matlab implementation of the 3GPP spatial channel model (3GPP TR 25.996)," *Jan*, 2005.
- [24] J. Max, "Quantizing for minimum distortion," *IRE Transactions on Information Theory*, vol. 6, no. 1, pp. 7–12, 1960.
- [25] S. Rangan, A. K. Fletcher, V. K. Goyal, and P. Schniter, "Hybrid generalized approximate message passing with applications to structured sparsity," in *IEEE International Symposium on Information Theory Proceedings (ISIT)*, pp. 1236–1240, IEEE, 2012.
- [26] N. Nagarajan, S. Koyejo, R. Ravikumar, and I. Dhillon, "Consistent binary classification with generalized performance metrics," in *Neural Information Processing Systems (NIPS)*, 2014.